J. Innovative Eng. Nat. Sci., vol. 5, no. 1, pp. 371-385, 2025.
http://doi.org/10.61112/jiens.1550755

JIENS
Journal of Innovative Engineering and Natural Science
(Yenilikçi Mühendislik ve Doğa Bilimleri Dergisi)
https://dergipark.org.tr/en/pub/jiens
Original Paper

Aeroelastic analysis of single–ply aramid and glass woven composite wing structures: numerical and experimental approaches

Mehmet Emre Oz [a,*], Bülent Ekici[a], Oguz Eryilmaz[b],

[a]Mechnaical Engineering, Marmara University, 34854, Istanbul, Turkey.
[b]Textile Engineering, Marmara University, 34854, Istanbul, Turkey.

ARTICLE INFO

Article history:
Received 16 September 2024
Received in revised form 22 December 2024
Accepted 24 January 2025

Available online

Keywords:
Aeroelasticity
Composite wing
Fluid-tructure interaction
Wind tunnel

ABSTRACT

Aeroelasticity involves the study of the interaction among aerodynamic, inertial, and elastic forces, where flutter manifests as a dynamic phenomenon, and divergence poses a static problem. Lightweight composite structures, that are lighter and stronger, have been studied in the current aviation industry for decades. In this study, aramid and glass plain woven single-ply composite wing structures were used in order to investigate aeroelastic interactions. The experimental and numerical comparisons of the aeroelastic responses of the wing structures were performed. Moreover, Ansys ACP was utilized to design the composite wing structure. The Fluid-Structure Interaction analysis was performed by using Ansys Fluent and Mechanical. The bending frequency responses of the wings were compared with each other at a different angle of attack (AoA) and different velocities (0 – 40 m/s). Operational Modal Analysis (OMA) was studied, and aerodynamic tests were performed using a subsonic wind tunnel to obtain the structural response of the composite wings. The flutter speed index (FSI) was determined for wings depending on the bending frequency. The aeroelastic results of computational and experimental methods for different composite wing structures were compared. The results show that the bending frequency of the aramid wing is higher than the glass wing. Also, the flutter speed index results for the aramid wing are in a safer region than the glass wing for different operational conditions.

I. INTRODUCTION

Composite materials are highly used in the aircraft industry because of their high strength-weight ratio, and they have different structural characteristics [1-4]. Various forms of composites exist, each with distinct mechanical and thermal properties [5-9]. Furthermore, modification processes are available for redesigning these material properties [10-12]. Alongside reconfiguration and using knows fibers (e.g. glass, aramid, carbon) laminating composite structures is a crucial process for determining mechanical characteristics [13-15]. Renowned for their high strength-to-weight ratio and design flexibility, composite materials have transformed the aerospace industry, facilitating the development of advanced structures. However, the dynamic interaction between composite materials and aerodynamic forces during flight introduces the complex phenomenon of aeroelasticity. In the aviation industry, there's an expectation for rapid solutions to aeroelastic analysis, yielding design results. Aeroelasticity involves the interaction among aerodynamic, inertial, and structural forces acting upon and within flight vehicle structures [16-18]. All structures deform when external loads are applied, but the loads and deformation interaction create aeroelastic problems, allowing separate analyses of static and dynamic behaviors [19-21]. Dynamic aeroelasticity or flutter involves the coupled solution of load and deformation occurring simultaneously [22]. Aeroelastic flutter is a hazardous phenomenon, potentially leading to a structure's total collapse. Predicting and eliminating aeroelastic flutter is crucial during the design and testing of aircraft and other structures. Various approaches, such as wind tunnel testing, computational simulations, and flight testing, are employed to determine flutter speed and flutter boundary, ensuring structural stability and

*Corresponding author. Tel.: +90-216-777-3730; e-mail: mehmetemreoz@gmail.com

safety [23, 24]. Applications for software like FLUENT and NASTRAN are crucial in the latest developments in aeroelasticity, simplifying and expediting processes compared to analytical approaches. Aeroelastic test techniques include airstream and non-airstream tests [25]. Non-airstream tests like ground vibration modes examine the dynamic behavior of the structure and forces acting on it at single or multiple points. Vibration modes are measured by scanning responses under different angle of attack (AoA) and free stream velocities, with natural frequencies changing based on loading conditions [26]. Several methods, including Operational Modal Analysis (OMA), are used to measure the natural frequency of a wing in a wind tunnel test. Operational Modal Analysis (OMA) is a method of determining the natural frequencies, or modal properties, of a structure by analyzing its response to operational loads [27], such as wind or vibration. OMA involves analyzing the wing's response to wind tunnel conditions, such as airflow, to determine natural frequencies. Frequency Domain Decomposition (FDD), a method of performing OMA, analyzes frequency content to extract modal properties [28]. The critical flutter speed ratio, sometimes referred to as the flutter speed ratio, quantifies the relationship between a structure's critical flutter speed and flutter speed. The crucial flutter speed is the lowest velocity where flutter speed becomes independent of structural damping, while flutter speed is the minimum velocity at which aeroelastic flutter occurs in the structure [29]. In aerospace engineering, the Flutter Speed Index (FSI) is a dimensionless number and a critical parameter that represents the ratio of the aircraft's operating speed to its flutter speed. It is used to evaluate the safety margin against aeroelastic instability. The flutter boundary is determined using subsonic flutter solution methods, such as the V-g method or the P-K method [18]. The airflow velocity at which flutter occurs is identified as the flutter speed, and the ratio of operating speed to flutter speed is referred to as the boundary. In this study, dynamic behavior is compared through both numerical simulations and experimental investigations.

This study involves experimental and numerical comparisons of aeroelastic responses in aramid and glass single-ply composite wing structures. Ansys ACP was used to design the composite wing structure, and Ansys Fluent and Mechanical conducted Fluid-Structure Interaction analysis. Bending frequency responses of the wings were compared at various angles of attack (AoA) and velocities (0–40 m/s). Operational Modal Analysis (OMA) and aerodynamic tests in a subsonic wind tunnel were performed to capture structural responses.

II. EXPERIMENTAL METHOD

2.1 Materials

In this study, a single-ply composite structure was employed to assess and compare the aeroelastic behavior of the composite wing. The internal construction part underwent standard investigation, while the wing surface was analyzed experimentally and numerically. The composite structure comprised two fundamental elements: the wing's internal part and the wing surface, which were composed of glass and aramid woven fabric for this study. Aramid composites generally exhibit higher stiffness characteristics compared to glass fiber composites [18]. Vacuum infusion is highly preferred by the aviation industry because of the applicable production process for different structural parts for instance wing, airframe, nosecone, and internal elements [19]. The composite wings in this study were manufactured using the vacuum infusion process (VIP). The wing molds, designed symmetrically, and the cestamite mold were crafted using CNC machining (Figure 1). The Torayca T300 Datasheet provides information on the fabric's volumetric mass. Polymer resin epoxy material properties were sourced from

the Ansys Datasheet, indicating a density of 1160 kg/m³. The wing's surface area measures 0.012 m², and both the aramid and the glass wing surfaces weigh 2.4 g and 2.52 g, respectively.

Table 1. Fabric properties for the construction of wings

Wing material	Aramid	Glass
Fabric Type	Plain woven fabric	Plain woven fabric
Weight (g/m^2)	200	210
Thickness (mm)	0.23	0.23

Figure 1. Mold system and vacuum infusion process of the wings

In the matrix system utilized for wing production, MGS L 160 epoxy resin and MGS H 160 hardener from HEXION company were chosen. The recommended mixing ratio of epoxy resin to hardener was 100:25 by weight, according to the manufacturer's instructions. Following the production of the composite wings, one surface of the aramid wing weighed 3.52 grams, while the glass wing weighed 3.57 grams (Figure 2). The volume of fibers within a composite volume is termed the fiber volume fraction, a crucial factor enhancing the composite's tensile characteristics. By considering the weights of the fibers and composite, along with the densities of the fibers and matrix, one can calculate this fraction using the "Rule of Mixture" [30]. The fiber volume fraction (FVF) of the wing structures is calculated from Equation (1).

$$v_f = \frac{\left(\frac{m_f}{d_f}\right)}{\left(\frac{m_f}{d_f}\right)+\left(\frac{m_r}{d_r}\right)} \quad (1)$$

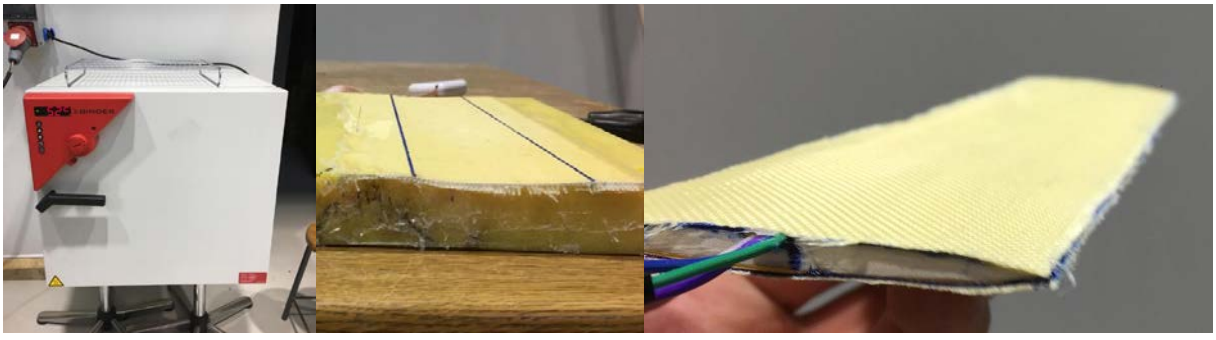

Figure 2. Composite wing manufacturing steps for the study (a) curing process (b) cutting process of surface (c) integration of upper and bottom wing surfaces

Where v_f is the fiber volume fraction (FVF), m_f is the weight of the fiber, d_f is the density of the fiber, m_r is the weight of the resin and d_r is the density of the resin. FVF is 0.68 for the aramid wing and 0.70 for the glass wing. Different methods exist for determining the fiber volume fraction (FVF) of a composite material, which is directly influenced by the processing method. In this study, the FVF exceeds 0.6 due to the use of a single-ply approach.

Table 2. Composite wing properties

Wing material	Aramid	Glass
Surface area of composite wing (m^2)	0.012	0.012
Fiber volume fraction	0.68	0.70

The wing structure consists of upper and bottom composite surfaces. Mechanical properties of the single-ply composite structures were obtained by using ASTM D3039 specimen dimensions. The mechanical properties are given in Table 3.

Table 3. Mechanical properties of aramid and glass for analyses

Material Type	Aramid	Glass
E_1 [GPa]	33.1	29.97
E_2 [GPa]	33.1	29.97
ν_{12}	0.28	0.225
ν_{21}	0.28	0.225
G_{12} [GPa]	3.61	4.98
G_{23} [GPa]	2.76	3.1
G_{13} [GPa]	2.76	3.1
ρ [kg/m^3]	1451	1930

Balsa was used the material of the wing construction elements and its mechanical properties are given in Table 4 [31]. Furthermore, balsa wood is inherently an orthotropic material; however, in this study, it is treated as an isotropic material due to the specific dimensions of the part being analyzed.

Table 4. Isotropic material properties

Material	Balsa	Epoxy
E [GPa]	3	4.3
G [GPa]	1.15	1.59
ν	0.3	0.35
ρ [kg/m^3]	130	1160

Geometrical parameters are important to investigate the flutter characteristics. In this study, NACA65A004 airfoil is analyzed, and it is a symmetrical airfoil, which does not produce the lifting force at zero angle of attack. The aeroelastic characteristics of the wing can be analyzed analytically.

A tapered leading-edge wing has been designed, with the geometrical dimensions outlined in Figure 3. These dimensions (AR= 4.44, λ =0.71) were selected considering wind tunnel testing conditions and constraints. Although the AGARD 445.6 wing is commonly preferred by aeroelasticians, its geometrical dimensions are not consistent for wind tunnel testing. To address this, a material with reduced torsional and bending stiffness, like balsa, was chosen. This choice was made due to stiffness considerations and experimental observations, as the flutter mechanism is significantly affected. Thus, balsa was selected as the material for spars and ribs. The configuration of the spars and ribs remained constant for each wing, while the composite wing surface was varied and compared in the study.

Internal support elements were bonded to the wing surface using pre-cured epoxy to complete the operation. The wing consists of two symmetrical upper and bottom surfaces, as shown in Figure 4. An accelerometer was positioned on the wing tip, and electronic signal cables were aligned along the wing ribs, nested for cable dimension.

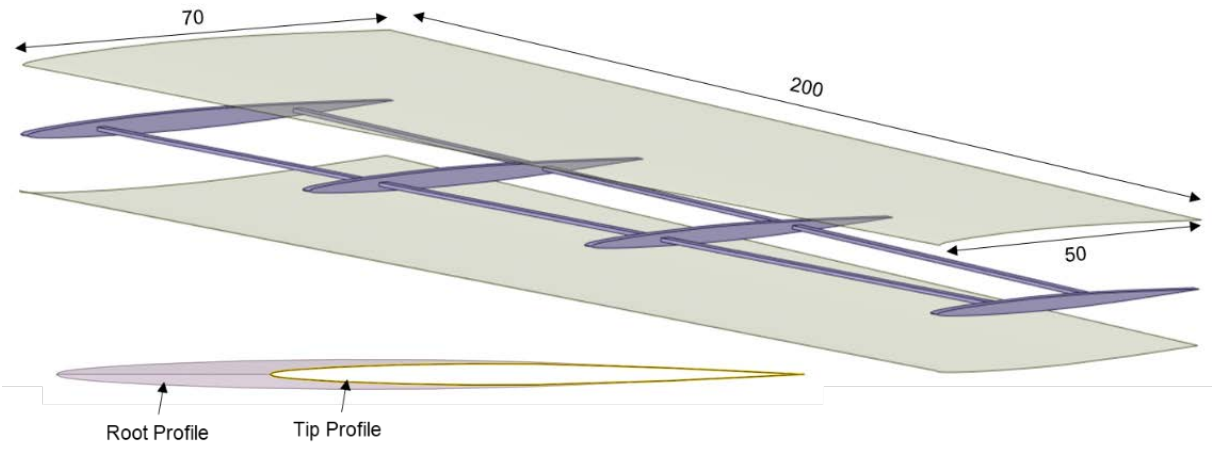

Figure 3. The dimensions and elements of the wing structure

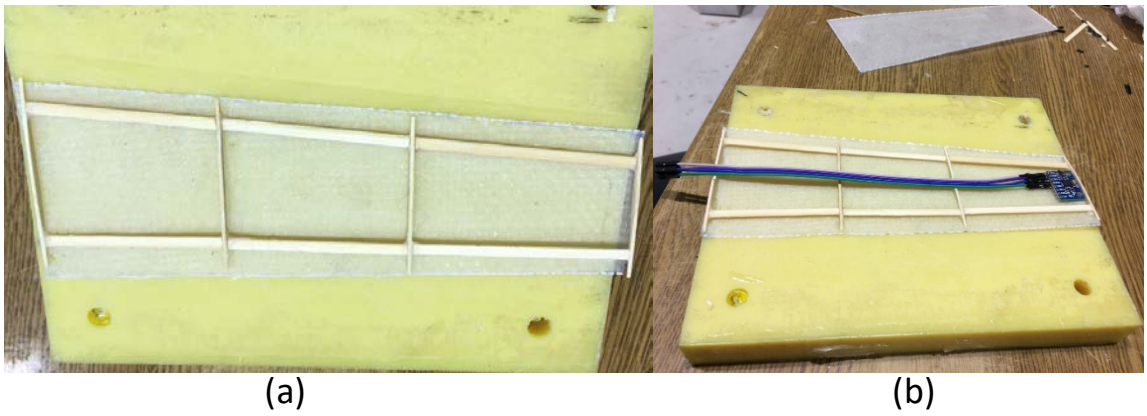

Figure 4. Wing structure (a) Rib-Spar Construction (b) Sensor integration

2.2 Computational method

Computational Fluid Dynamics (CFD) simulations were conducted using Ansys Fluent and Mechanical. The flow field around the wing was analyzed at a specific angle of attack and freestream velocity through Fluid-Solid Interaction analysis. Modal analysis was employed to identify the natural frequencies and mode shapes of the wing structure, utilizing pressure distribution on the wing surface obtained from the CFD study as a loading condition [22]. This facilitated a comprehensive Fluid-Structure Interaction analysis, providing significant insights into how the wing's structural response to aerodynamic loads influences fluid flow [23, 24]. Additionally, the performance and stability of two composite wing structures were compared under various aerodynamic conditions. The natural frequency and flutter behavior of both wings were analyzed using modal frequencies derived from the modal analysis [25]. To validate the simulation, findings were cross verified with results from wind tunnel tests.

Composite wing surface layers were designed in Ansys ACP, considering fiber orientation's direct impact on structure stiffness [26]. The wing's vibration characteristics were studied in a subsonic wind tunnel, aligning the aerodynamic model with experimental conditions and flow considerations such as flow separation and intensity. The Reynolds Number was 5x105, indicating turbulent flow in the aerodynamic experiment. Pressure-based CFD analysis utilized the k-omega SST viscosity model for the ideal gas representing air. A fine mesh was employed near the wing, while a coarse mesh optimized solution time for regions farther from the wing-body. The dynamic characteristics of the wing, specifically its behavior under aerodynamic load, were investigated, with a focus on flutter phenomena—the non-damped oscillations of an aerostructure caused by aerodynamic forces [25]. Numerical analysis of wing responses under different airspeeds and angles of attack was carried out using fluid-structure interaction. The computational model of the composite structure in Ansys provided structural frequencies under airflow. Pressure data was transferred to the structural model, treating the wing materials as fluid-structure, and modal analysis was conducted with pre-stress. Frequency responses were investigated in harmonic analysis using transferred modal and structural environments. The mechanical and fluid models are coupled and solved simultaneously. A time step of 0.01 seconds is used for each model's overlapping solution period. In this solution, the computational system operates at a frequency of 100 Hz, ensuring that the natural frequency remains within the required range.

The mode shapes for each wing exhibited similar characteristics in structural analysis. An example of mode shapes (bending, twisting, or coupled) for the aramid composite wing is provided in Figure 5, with both calculated natural frequencies shown in Table 5.

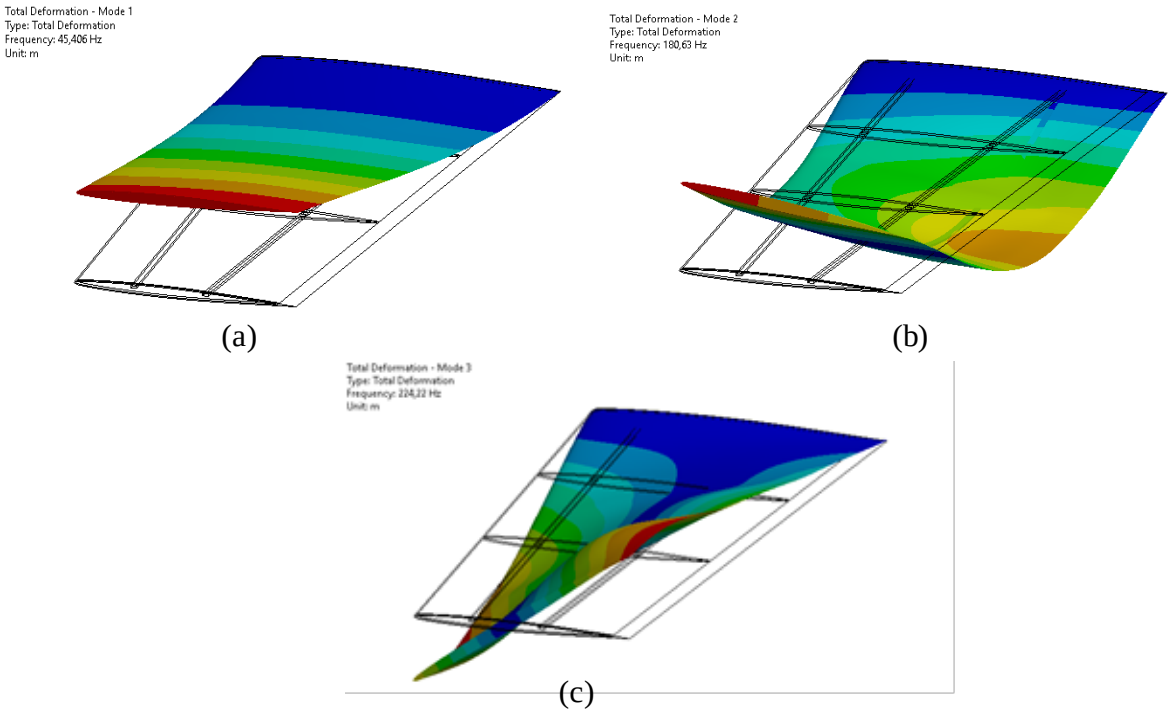

Figure 5. Composite wing calculated natural frequencies (a) Mode 1, first bending (b) Mode 2, second bending (c) Mode 3, first twisting

Table 5. The natural frequencies of aramid and glass wings

Mode	Aramid (Hz)	Glass (Hz)
1	45.648	39.076
2	180.63	167.07
3	224.22	262.08

The natural frequencies of the wing structures reveal the characteristics of their bending and twisting modes. Figure 5 illustrates the mode shapes and corresponding natural frequencies of the aramid wing. A comparable trend is observed in the frequency variations of both wings.

The flutter boundary serves as a criterion for the system's response when it becomes neutrally stable, signifying neutral response occurrence. When the speed index falls below the critical value on the flutter boundary, both displacements and lift coefficient decay, indicating a damped response [32]. The typical behavior of the flutter boundary is illustrated concerning the Mach number. The system exhibits neutral oscillation response when the flutter speed index (FSI) closely approaches the critical value of the boundary [33]. The system is stable when FSI is below the critical value. Otherwise, the response of the system is diverge periodically when FSI is beyond the critical value [34].

$$FSI = \frac{U_\infty}{b\omega\sqrt{\mu}} \tag{2}$$

$$\mu = \frac{m}{\pi b^2 \rho l} \tag{3}$$

FSI is calculated as $U_\infty$is free stream velocity, b is half-chord length, ω is structural frequency, μ is the mass ratio, m is wing mass, ρ is the density of free stream, l is the length of the wing. For the composite wing structures, flutter index numbers were obtained by using Equation 2 and 3 [34]. In the experiment, fluid flow was incompressible. The flutter point was then measured in air at a Mach number less than 1 M, with the corresponding flutter calculation based on the mass and stiffness properties of the model tested and on the experimental values of Mach number and flow density [35].

2.3. Experimental method

The aeroelastic behavior of two composite wing structures was examined in a subsonic wind tunnel, covering various speeds and angles of attack (AoA). Accelerometers were attached to the tips of each wing to monitor their responses during wind tunnel tests. Operational Modal Analysis (OMA), specifically Frequency Domain Decomposition (FDD), was employed to gain insights into how the structures behaved under different operational conditions. Frequency Domain Decomposition (FDD) is a technique used to transform collected acceleration data from the time domain into the frequency domain. This method is applied to experimental datasets to determine natural frequencies through Operational Modal Analysis (OMA), a technique for identifying modal parameters. To understand the modal characteristics of the wings across varying wind speeds and AoAs, accelerometer data were collected and analyzed using FDD, providing accurate estimations of natural frequencies and modal

parameters. Given the potential for structural failure during testing, which could harm both the tunnel mechanism and test devices, the experimental conditions were carefully controlled. The operational conditions that could lead to flutter states causing damage within the tunnel were avoided. Specifically, to prevent instability and excessive deflection due to total pressure on the wing, the freestream velocity was restricted for AoA values of 5° and 10°, mitigating potential structural issues. The primary objective of the aeroelastic test was to validate the dynamic behavior of an elastic mechanical system under aerodynamic conditions. Figure 6 illustrates the experimental setup and the subsonic wind tunnel used for these investigations.

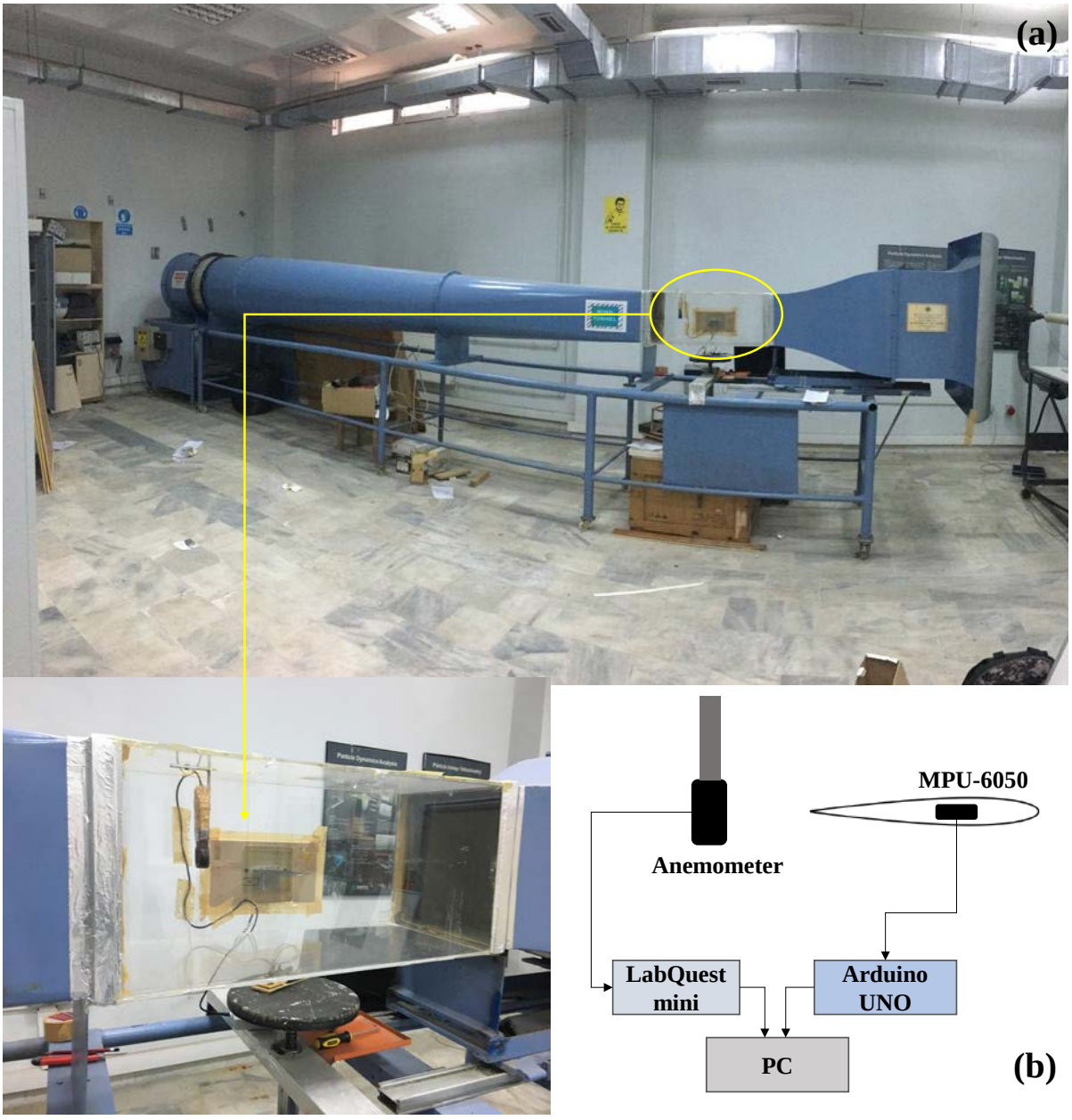

Figure 6. (a) Subsonic wind tunnel used for the study and (b) experimental setup of the data collection

During the wind tunnel test, accelerometer data were acquired from the MPU 6050, equipped with three linear axes and three rotational axes. Bending motion data of the wing was recorded in the time domain. The test was repeated

five times, with each iteration lasting sixty seconds and including the acceleration dataset. The accelerometer operated at a frequency of 50 Hz. Aerodynamic tests were conducted at various angles of attack, recognizing that aerodynamic load increases with flow velocity. However, there are conditions where the combination of angle of attack and structural resistivity of the wings might not be sufficient to withstand external loads. In such cases, aero tests were concluded within the range of wing structural capabilities. Testing was carried out up to 20 m/s and 15 m/s for AoA = 5° and AoA = 10°, respectively. In this study, the Frequency Domain Decomposition (FDD) method for Operational Modal Analysis (OMA) was employed to gather response data from a composite wing structure using an accelerometer. To discern the modal characteristics of the wing under various freestream velocities and angles of attack, acceleration measurements were taken at a single location on the structure. The data, formatted for recognition by the Arduino, was transferred to MATLAB for the subsequent FDD analysis.

III. RESULTS AND DISCUSSIONS

3.1 Bending Frequencies

The experimental and computational behavior of the composite wing was scrutinized, and the system's response was obtained in the frequency domain. A comparative analysis between numerical and experimental results has been visually presented, revealing a noticeable correlation in the frequency trends. Figure 7 illustrates the bending frequencies for the aramid wing, providing a clear representation of the concordance between numerical predictions and experimental observations.

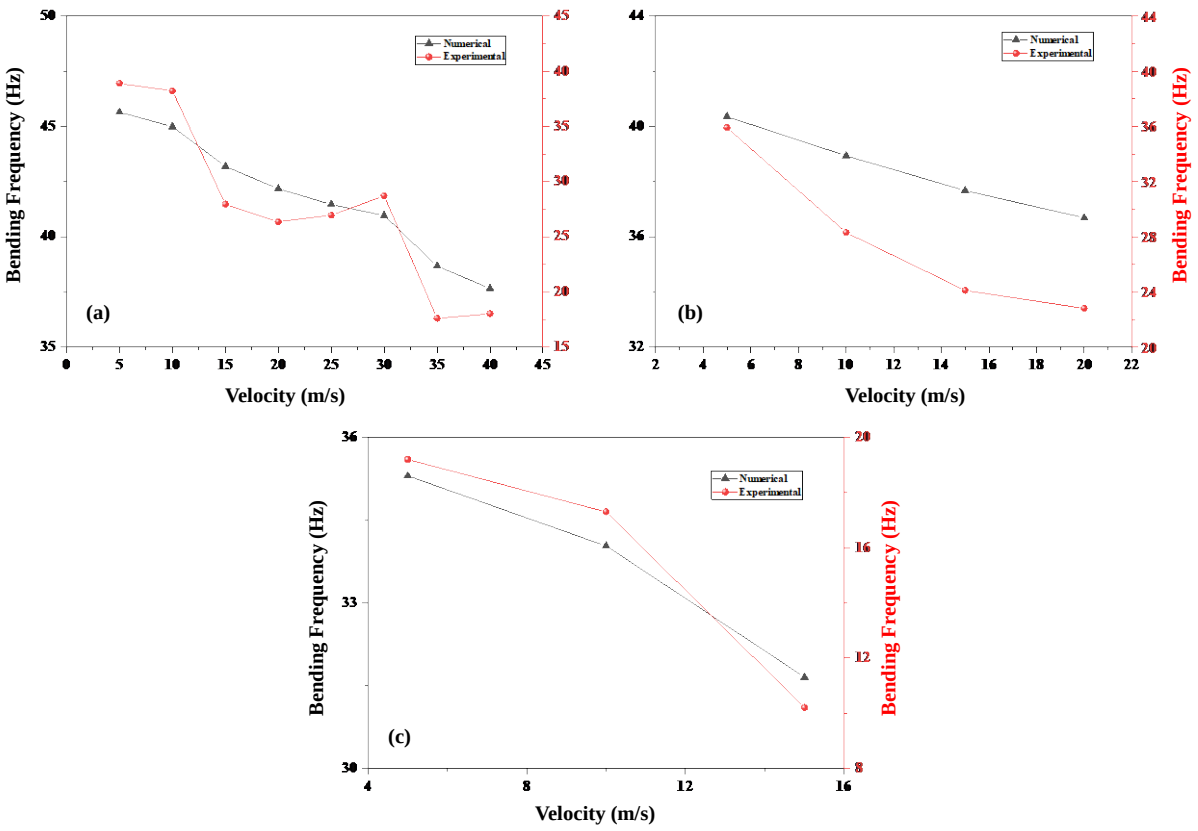

Figure 7. Bending frequencies of aramid wing at (a) AoA=0°, (b) AoA=5°, and (c) AoA=10°

A variance in numerical frequencies was noted, primarily due to the negligible impact of external factors on the structural system. The freestream velocity range exhibited subtle changes, resulting in an expected small variation in natural frequencies for the aerodynamically loaded wing [36]. There is not a difference between numerical and experimental frequency outcomes which is not much. However, after 15 (m/s) this difference increased by about a factor of 2. The maximum numerical bending frequencies were identified as 45.648 Hz and 39.076 Hz, while the maximum experimental frequencies were recorded at 38.89 Hz and 32.50 Hz for the aramid and glass wings, respectively. At AoA = 0°, the numerical decrement is approximately 17.51% and 21.44% for the aramid and glass wings, respectively. This rises to 9.09% and 15.15% at AoA = 5°, and further to 10.34% and 10.75% at AoA = 10° for the aramid and glass wings, respectively. On the other hand, the experimental analysis shows more variations at AoA = 0° (53.68% and 60.15%), AoA = 5° (36% and 51.28%), and AoA = 10° (46% and 33%) for aramid and glass wings, respectively. The experimental results align with the anticipated trends observed in numerical simulations. For the aramid wing, a consistent decrease in bending frequency is noted with increasing freestream velocity. The frequency remains stable between 5 and 25 m/s for AoA = 0° in the numerical analysis results. However, in the experimental analysis, a steady behavior is observed from 15 to 25 m/s, with a deviation in frequencies between 10 and 15 m/s. Similar downward trends are apparent at AoA = 5° and 10° in both numerical and experimental results. The choice of accelerometer and measurement points significantly influences frequency determination. Limited data collection at the wing's tip in this study may have contributed to observed differences and impacted experimental results.

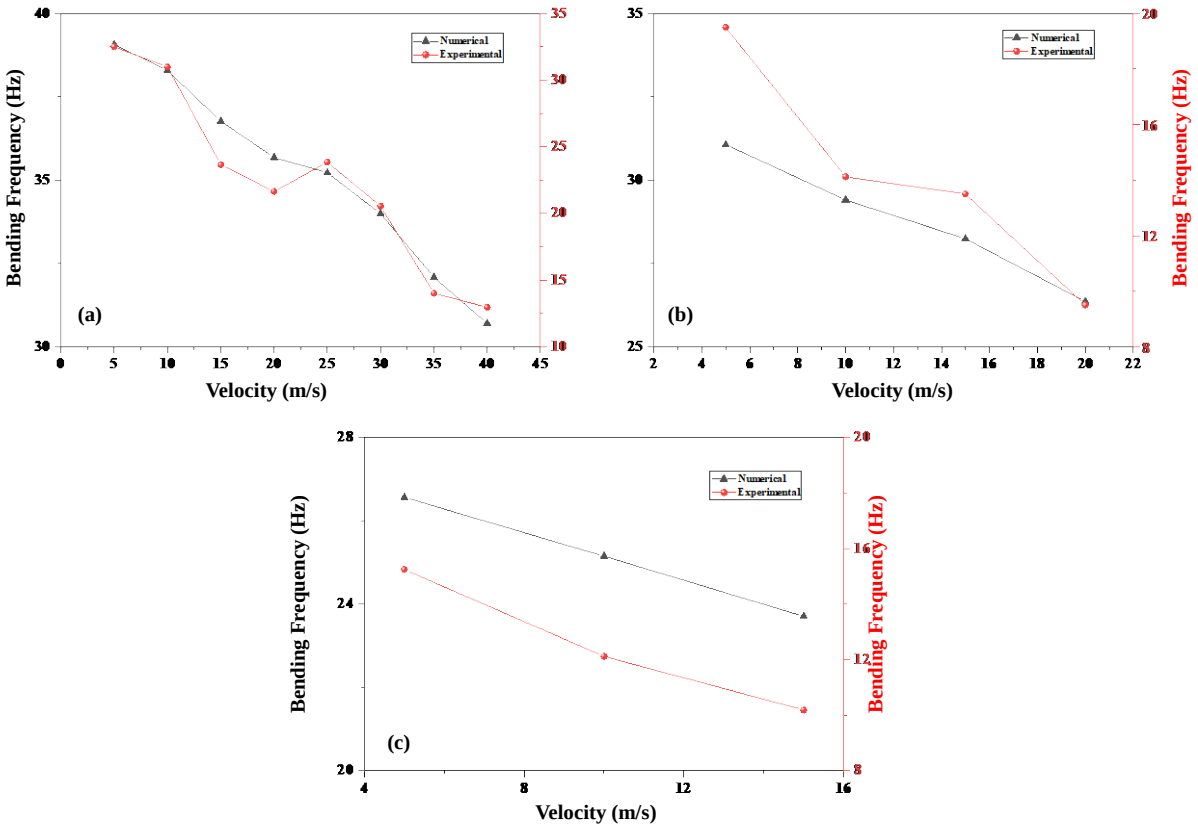

Figure 8. Bending frequencies of glass wing at (a) AoA=0°, (b) AoA=5°, and (c) AoA=10°

The bending frequencies of the glass wing, under different angles of attack (AoA = 0°, 5°, 10°), are illustrated in Figure 8, comparing numerical and experimental results. At AoA = 0°, a frequency decrease is evident in both numerical and experimental outcomes. The decrement rate continues for AoA = 5° and 10°, with the change in aerodynamic loading exerting a more pronounced influence. The bending frequency maintains a steady behavior at AoA = 0° between 10 and 30 m/s, where numerical and experimental frequencies exhibit concordant decreases at the same freestream velocities. However, a degree of irregularity is observed in the numerical result at AoA = 0°, which contrasts with the steadier trend observed at AoA=5° and 10°. This suggests that the aerodynamic effects were more ideal in the computational model, while structural deformities and irregularities in the flow caused frequency deviations in the aerodynamic load [37]. The bending frequency is contingent on external load, nodal mass, and stiffness properties of the structure, decreasing as both the angle of attack and freestream velocity increase [32]. Behaviors at different operational angles of attack and velocities are depicted in Figure 9 and 10.

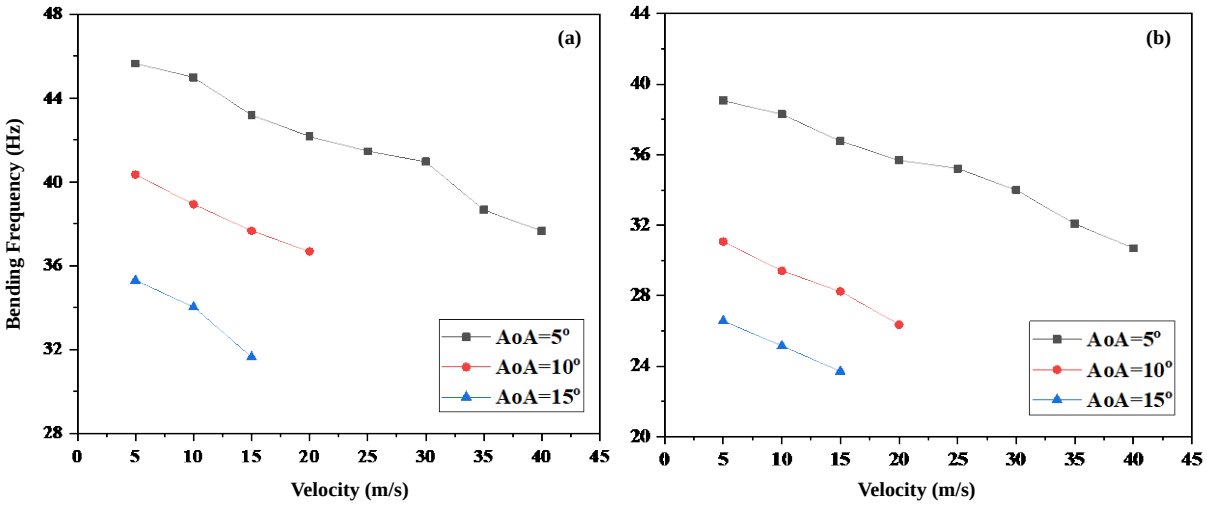

Figure 9. Numerical bending frequency results; (a) aramid wing (b) glass wing

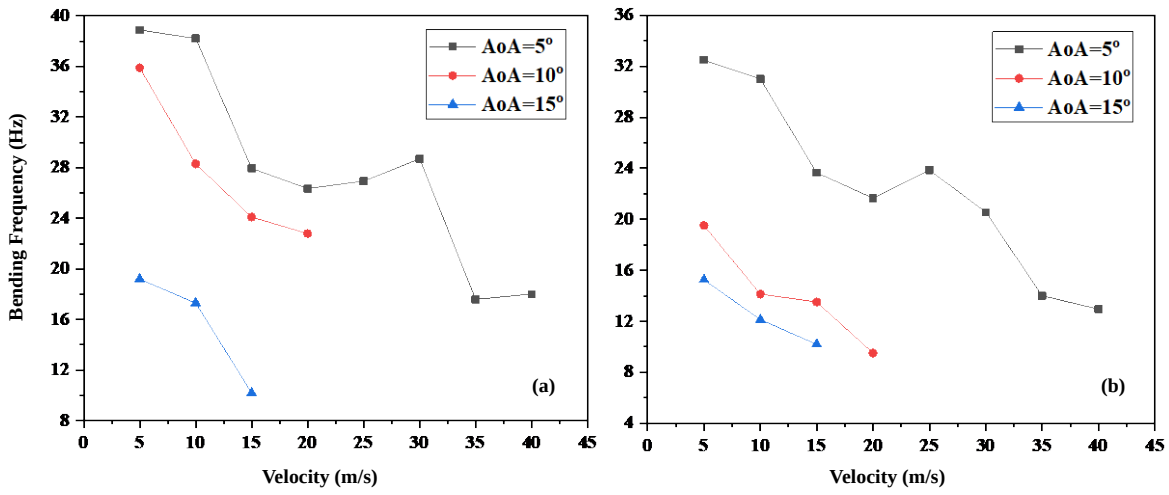

Figure 10. Experimental bending frequency results: (a) aramid wing (b) glass wing

In the numerical results for both wing structures, the bending frequency tends to remain steady up to 30 m/s at AoA = 0°. The experimental results, as shown in Figure 10 up to 30 m/s, indicate that the frequency resists continuous decline. However, a specific frequency decrease is observed in both wings within the range of 10 to 15 m/s. This may be attributed to the operating frequency of the flow-generating motor at those speeds in the wind tunnel. The slope of the bending frequency increases relatively with the angle of attack. At an angle of attack of 5°, the aramid wing experiences a less dramatic decline in bending frequency compared to the glass wing, which undergoes a considerable drop at 20 m/s, both numerically and experimentally. Between an angle of attack of 5° and 10°, a higher drop rate is observed in the aramid wing, while the drop rate is lower in the glass wing.

3.2 Flutter Speed Index

Flutter Speed Index (FSI) values were calculated for different wing structures with bending frequencies (Figure 11) in terms of flutter characteristics of the wing structure.

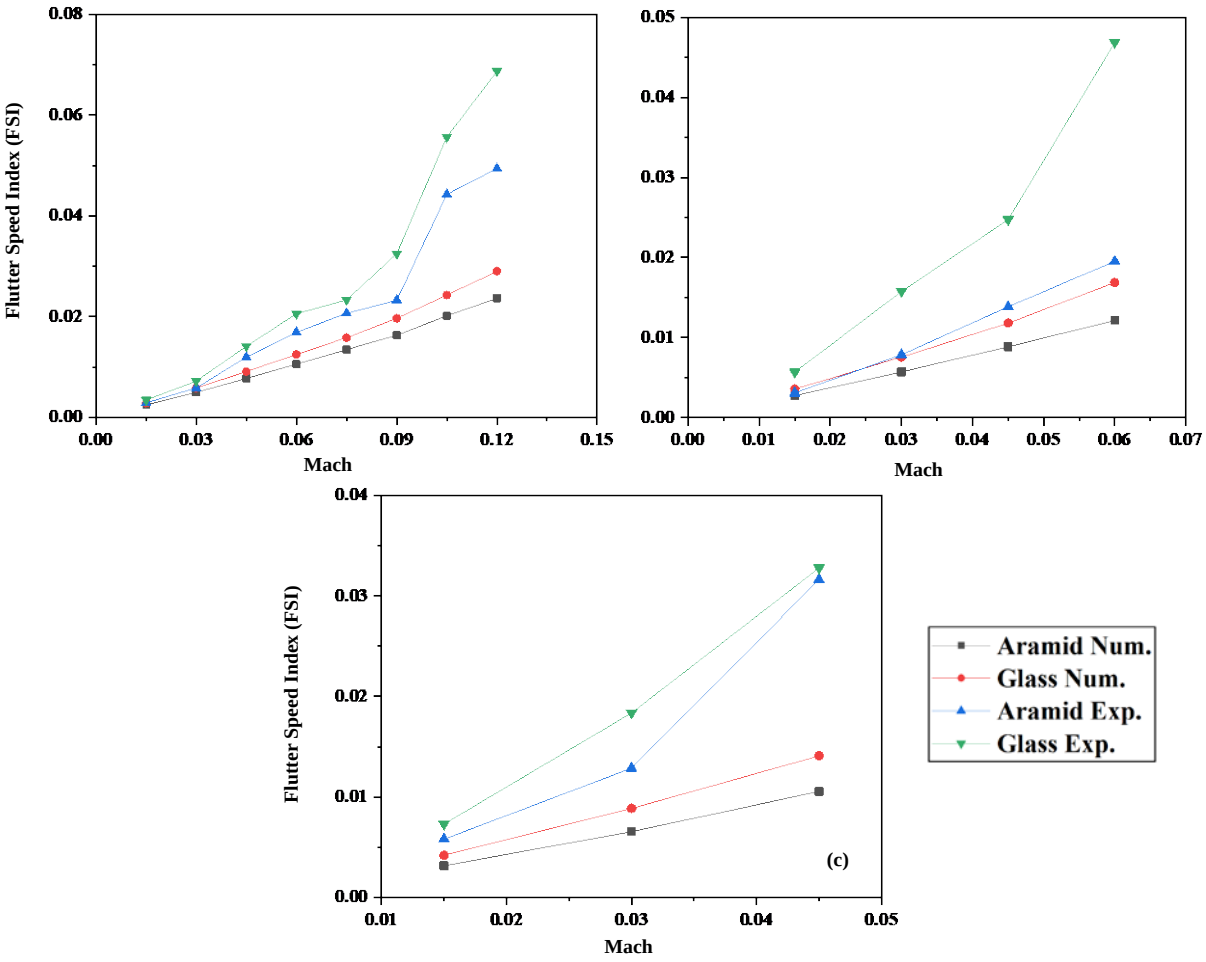

Figure 11. Numerical FSI results of at (a) AoA=0°, (b) AoA=5°, and (c) AoA=10°

The FSI values being far from the flutter boundary indicates that the wing structures are in a safe zone for operational flight conditions. In this study, FSI values are below the flutter boundary. A key finding is that the

aramid wing provides lower FSI values than the glass wing in both numerical and experimental methods. In the numerical analysis results, linear behavior in FSI values is observed. However, the experimental analysis results of FSI values exhibit non-linear behavior due to the fluctuation and sudden change in bending frequencies. In contrast to experimental results, computational outcomes are free from defects and imperfections. Experimental limitations arise due to assumptions, manufacturing processes, testing conditions, and data processing, leading to variations in the amplitude of experimental results. Additionally, the experimental analysis results are higher than the numerical analysis results, as the bending frequencies in the experimental results are lower than the numerical results of the FSI number, exhibiting a sixfold difference between them. In conclusion, considering the response of the wing in the experiment, the flutter characteristics of the wing structure, based on bending frequency consideration, do not show a decrement in the FSI in both experimental and computational methods. Therefore, the structure is stable for aeroelastic test conditions. Comparatively, the NACA0012 Benchmark model studied by Rivera in the NASA Technical Report for subsonic flight conditions demonstrated a downtrend in bending frequency from 4.56 Hz to 4.07 Hz with increasing velocity [38]. Similar methodologies were employed by Khatir, T., et al. [39], indicating a downtrend in bending frequency concerning increasing freestream velocities in the subsonic range (up to 40 m/s).

IV. CONCLUSIONS

Composite wing structures, reinforced with aramid and glass fibers and featuring the NACA65A004 section profile, underwent modeling to validate their natural frequencies. An aeroelastic experiment was conducted in a subsonic wind tunnel to explore the structure's response to aerodynamic loading. With the primary goal of comparing composite wings, other material parameters (cohesive and internal elements) were held constant. The analysis focused on discerning frequency behavior based on the surface material of the wing. The general trends of the bending frequency in both numerical and experimental results are correlated. As the initial angle of attack increases, bending frequencies of the composite wings, both numerically and experimentally, decrease. This decrease is also observed with an increase in the angle of attack, influenced by changes in aerodynamic loads and turbulent flow on the wing surface. Also, it needs to be taken account that the choice of accelerometer for collecting bending acceleration, and the number of measurement points influence frequency determination. In this study, data collected from a single point at the wing's tip might have contributed to the observed subtle differences and decreases in experimental analysis results. Furthermore, there is a decrease in bending frequency with an increase in freestream velocity. The bending frequency of the aramid wing is consistently higher than that of the glass wing for different angles of attack ($\alpha=0°$, $\alpha=5°$, and $\alpha=10°$). In terms of the flutter speed index (FSI), the aramid wing results in a safer region than the glass wing, as the bending frequency of the aramid wing is higher than that of the glass wing. Additionally, it was observed that as velocity increased in both numerical and experimental scenarios, the margin between the flutter regions of aramid and glass wings increased. The performance of the aramid wing structure is deemed more reliable due to the greater bending stiffness of aramid compared to glass. The longitudinal elasticity modulus of the orthotropic material could affect stiffness, and this can be optimized by changing the orientation of the fiber lamination. Verification and validation are essential in aerospace engineering design. Experimental data plays a critical role in analyzing aircraft components and validating numerical models. With the

rising use of low speed unmanned aerial vehicles (UAVs), the demand for aeroelastic experimental data is increasing. Future research will prioritize creating dynamic models of wing structures using experimental datasets.

ACKNOWLEDGMENT

This study has been supported and funded by the Scientific and Technological Research Council of Turkey (TÜBİTAK) 2209-A Program. The authors would like to acknowledge the support provided by Marmara University Faculty of Engineering and Technology as well as Thermo-Fluid Testing Laboratory.

REFERENCES

1. Eryilmaz O, Sancak E (2021) Effect of silane coupling treatments on mechanical properties of epoxy based high-strength carbon fiber regular (2 x 2) braided fabric composites. Polymer Composites 4212:6455-6466. https://doi.org/10.1002/pc.26311
2. Eryilmaz O et al (2024) FEA and experimental ultimate burst pressure analysis of type IV composite pressure vessels manufactured by robot-assisted radial braiding technique. Int Journal of Hydrogen Energy 50:597-612. https://doi.org/10.1016/j.ijhydene.2023.07.302
3. Eryilmaz O, Kocak ED, Sancak E (2023) 8-Braided natural fiber preforms. Mohamad M (ed) Multiscale Textile Preforms and Structures for Natural Fiber Composites. Woodhead Publishing, pp 221-237. https://doi.org/10.1016/B978-0-323-95329-0.00007-7
4. Yildiz Z, Eryilmaz O, (2023) 12-Preimpregnated natural fiber preforms. Mohamad M (ed) Multiscale Textile Preforms and Structures for Natural Fiber Composites. Woodhead Publishing, pp 327-340. https://doi.org/10.1016/B978-0-323-95329-0.00003-X
5. Eryilmaz O (2024) Revalorization of cellulosic fiber extracted from the waste stem of Brassica oleracea var. botrytis L. (cauliflower) by characterizing for potential composite applications. Int Journal of Biological Macromolecules 266:131086. https://doi.org/10.1016/j.ijbiomac.2024.131086
6. Eryilmaz O et al (2020) Investigation of the Water–Based Ink Hold onto the Thermoplastic Composites Reinforced with Sisal Fibers. Journal of Textile Science Fashion Technology 53. https://dx.doi.org/10.33552/JTSFT.2020.05.000612
7. Sen M, Eryilmaz O, Bakir B (2024) Micro drilling characterization of the carbon and carbon–aramid (hybrid) composites. Polymer Composites 456:5449-5459. https://doi.org/10.1002/pc.28138
8. Öz M, Yıldırım Y, Eryılmaz O (2021) Investigation of Spacer Fabric as Vibration Reduction Material in Rocket Avionic Systems by Using Finite Element Method. in 8. International Fiber and Polymer Research Symposium (8. ULPAS). Eskişehir.
9. Sen M, Eryilmaz O, Bakir B (2024) Multi-objective Process Optimization of Micro-drilling Parameters on Carbon and Carbon–Aramid (Hybrid) Fabric Composites. Arabian Journal for Science and Engineering. https://doi.org/10.1007/s13369-024-09616-z
10. Eryılmaz O, Ovalı S (2024) Investigation and Analysis of New Fiber from Allium fistulosum L. (Scallion) Plant's Tassel and its Suitability for Fiber-Reinforced Composites. Uludağ Üniversitesi Mühendislik Fakültesi Dergisi 291:51-66. https://doi.org/10.17482/uumfd.1410520
11. Ovalı S, Eryılmaz O (2024) Physical and Chemical Properties of a New Cellulose Fiber Extracted from the Mentha pulegium L. (Pennyroyal) Plant's Stem. Çukurova Üniversitesi Mühendislik Fakültesi Dergisi 391:211-220. https://doi.org/10.21605/cukurovaumfd.1460444
12. Ovalı S, Eryılmaz O, Uyanık S (2024) Exploring the potential of sustainable natural cellulosic fiber from Sorghum bicolor (Sorghum vulgare var. technicus) stem for textile and composite applications. Cellulose 31:3289-3302. https://doi.org/10.1007/s10570-024-05800-4
13. Eryılmaz O (2022) Havacılık taşıtlarındaki uygulamalar için karbon lif takviyeli kompozit yüksek basınç/yakıt tankı tasarımı ve üretimi. Dissertation, Marmara University.
14. Eberhardt B et al (2022) Inline contactless optical measuring of glass fiber properties and retrofitting an adaptive cooling system for glass fiber production. in Aachen Reinforced. Aachen, Germany
15. Eryılmaz O et al (2020) Elyaf Sarma Yöntemi ile Üretilmiş Cam Lifi Takviyeli Kompozit Roket Gövdesinin Paraşüt Mekanizmasının FR Kumaşlar ile Yalıtılması. in Uşak Üniversitesi TTO 1.Ar-Ge ve Tasarım Proje Pazarı. Uşak, Türkiye
16. Mukhopadhyay V (2003) Historical Perspective on Analysis and Control of Aeroelastic Responses. Journal of Guidance, Control, and Dynamics 265:673-684. https://doi.org/10.2514/2.5108

17. Irani S, Sazesh S (2013) A new flutter speed analysis method using stochastic approach. Journal of Fluids and Structures 40:105-114. https://doi.org/10.1016/j.jfluidstructs.2013.03.018
18. Eryilmaz O, Öz M (2023) Aeroelastic Analysis of the Composite Wing Reinforced with Carbon Fiber. in Çankaya International Congress on Scientific Research. Ankara
19. Fagley C, Seidel J, McLaughlin T (2016) Cyber-physical flexible wing for aeroelastic investigations of stall and classical flutter. Journal of Fluids and Structures 67:34-47. https://doi.org/10.1016/j.jfluidstructs.2016.07.021
20. Scanlan RH (2000) Motion-Related Body-Force Functions in Two-Dimensional Low-Speed Flow. Journal of Fluids and Structures 141:49-63. https://doi.org/10.1006/jfls.1999.0252
21. Peters DA (2008) Two-dimensional incompressible unsteady airfoil theory—An overview. Journal of Fluids and Structures 243:295-312. https://doi.org/10.1016/j.jfluidstructs.2007.09.001
22. Murua J, R Palacios, JMR Graham (2012) Applications of the unsteady vortex-lattice method in aircraft aeroelasticity and flight dynamics. Progress in Aerospace Sciences 55:46-72. https://doi.org/10.1016/j.paerosci.2012.06.001
23. Chai Y et al (2021) Aeroelastic analysis and flutter control of wings and panels: A review. International Journal of Mechanical System Dynamics 11:5-34. https://doi.org/10.1002/msd2.12015
24. Li W et al (2007) Thermal flutter analysis of large-scale space structures based on finite element method. International Journal for Numerical Methods in Engineering 695:887-907. https://doi.org/10.1002/nme.1793
25. Sundresan M et al (2012) Review of Aeroelasticity Testing Technology. Procedia Engineering 38:2297-2311. https://doi.org/10.1016/j.proeng.2012.06.276
26. Pagani A et al (2021) Static and dynamic testing of a full-composite VLA by using digital image correlation and output-only ground vibration testing. Aerospace Science and Technology 112, 106632. https://doi.org/10.1016/j.ast.2021.106632
27. Aenlle ML, Brincker R (2013) Modal scaling in operational modal analysis using a finite element model. International Journal of Mechanical Sciences 76:86-101. https://doi.org/10.1016/j.ijmecsci.2013.09.003
28. Jianghua G et al (2018) Dynamic analysis of laminated doubly-curved shells with general boundary conditions by means of a domain decomposition method. International Journal of Mechanical Sciences 138:139:159-186. https://doi.org/10.1016/j.ijmecsci.2018.02.004
29. Gallman JW, Batina JT, Yang TY (1988) Computational transonic flutter boundary tracking procedure. Journal of Aircraft 253:263-270. https://doi.org/10.2514/3.45587
30. Noroozi M, A Zajkani, M Ghadiri (2021) Dynamic plastic impact behavior of CNTs/fiber/polymer multiscale laminated composite doubly curved shells. International Journal of Mechanical Sciences 195, 106223. https://doi.org/10.1016/j.ijmecsci.2020.106223
31. Rumayshah KK, Prayoga A, Agoes Moelyadi M (2018) Design of High Altitude Long Endurance UAV: Structural Analysis of Composite Wing using Finite Element Method. Journal of Physics: Conference Series 10051, 012025. https://doi.org/10.1088/1742-6596/1005/1/012025
32. Yuan W, Sandhu R, Poirel D (2021) Fully coupled aeroelastic analyses of wing flutter towards application to complex aircraft configurations. Journal of Aerospace Engineering 342, 04020117. https://doi.org/10.1061/(ASCE)AS.1943-5525.0001232
33. Marques AN et al (2020) Multifidelity Method for Locating Aeroelastic Flutter Boundaries. AIAA Journal 584:1772-1784. https://doi.org/10.2514/1.J058663
34. Chaitanya J et al (2017) Vibrational characteristics of AGARD 445.6 wing in transonic flow. in IOP Conference Series: Materials Science and Engineering. India.
35. Dowell E H et al (1989) Unsteady transonic aerodynamics and aeroelasticity. Howard C (ed) A modern course in aeroelasticity. Springer Netherlands:Dordrecht, pp 443-501. https://doi.org/10.1007/978-94-015-7858-5_9
36. Theodorsen T (1979) General Theory of Aerodynamic Instability and the Mechanism of Flutter. NASA Ames Research Center Classical Aerodynamics Theory pp 291-302.
37. Jan R et al (2014) Aeroelasticity and Loads Models. Jan R (Ed) Introduction to Aircraft Aeroelasticity and Loads, pp 465-474. https://doi.org/10.1002/9781118700440.ch21
38. Rivera J et al (1992) NACA 0012 benchmark model experimental flutter results with unsteadypressure distributions. in 33rd Structures, Structural Dynamics and Materials Conference. Dallas.
39. Khatir T et al (2017) Experimental and numerical investigation of flutter phenomenon of an aitcraft wing (NACA 0012). Mechanics 234:562-566. https://doi.org/10.5755/j01.mech.23.4.15175